Journal of Membrane Science 637 (2021) 119635

Contents lists available at ScienceDirect

Journal of Membrane Science

journal homepage: www.elsevier.com/locate/memsci

Large-pore covalent organic frameworks for ultra-fast tight ultrafiltration (TUF)

Siyu Fang, Xiansong Shi **, Xingyuan Wang, Zhe Zhang, Congcong Yin, Zhipeng Zhang, Tong Ju, Sen Xiong ***, Yong Wang *

State Key Laboratory of Materials-Oriented Chemical Engineering, College of Chemical Engineering, Nanjing Tech University, Nanjing, 211816, Jiangsu, PR China

ARTICLE INFO

Keywords:
Large-pore COFs
Tight ultrafiltration
Unidirectional diffusion
Molecular separation
Dye/salt separation

ABSTRACT

Tight ultrafiltration (TUF) membranes featuring specific pore sizes are increasingly developed to bridge the gap between nanofiltration and ultrafiltration. So far, a wealth of efforts has been devoted to tackle the limitation found in TUF, but there still lacks a facile accessibility to upgrade TUF membranes with simultaneously improved permeance and selectivity. Herein, we report a large-pore covalent organic framework (LP-COF) as the building material to prepare ultra-permeable TUF membranes for fast separations. The LP-COF layers with an exceptionally large aperture size of up to ~3.6 nm are synthesized on macroporous substrates through a unidirectional diffusion method. The resultant LP-COF layers show a moderate crystallinity and low thickness down to ~60 nm, and allow ultrafast water permeation. Surprisingly, the optimal LP-COF membrane exhibits an unprecedented water permeance of ~3147 L m^{-2} h^{-1} MPa^{-1} with a high Congo red rejection (~92.6%), which is basically unchanged after several cycles of filtration. Moreover, the large-pore channels enable an unimpeded pass of ions, thus affording the membrane an excellent dye/salt separation competence, and largely exceeding state-of-the-art membranes. Therefore, this work opens up a new opportunity in producing high-performance TUF membranes by large-pore COFs for rapid and precise separations.

1. Introduction

Molecular separation in liquid environment exemplified by polypeptide fractionation, extraction of active pharmaceutical ingredients and textile wastewater treatment is promising to selectively recover targeted molecules from mixtures [1–3]. In the past decade, ever-growing demand for a cost-effective technology to produce high-quality molecular products urges the emergence of various strategies [4]. Compared with conventional separation methods, membrane-based technology is considered as one of the excellent platforms to implement this task, owing to the advantages of flexible operation, high efficiency and small environmental footprint [5]. Among current membrane technologies, nanofiltration (NF) and ultrafiltration (UF) have demonstrated their superiorities in the separation and purification of molecular objects from aqueous and organic solutions. For instance, considerable achievements have been made in the pharmaceutical engineering by using NF membranes [6]. However, in spite of the desired separation precision, the operation efficiency of them is largely limited due to the relatively low permeance. Recently, the modification strategies in terms of microstructures and surface properties have been suggested to break through this limitation, yet these studies mostly concentrated on the desalination instead of molecular separation [7–9]. As for traditional UF membranes, they are perfect in the separation of large molecules likes proteins and nano-sized particles [10–12], while giving a remarkable water permeance. Nevertheless, the majority of UF membranes possess large pore sizes (typically ~10–100 nm), which may hamper them from being used in the separation of small molecules, especially in the range of 2–5 nm. In order to meet the separation requirement in this range, tight UF (TUF) membranes featuring mesopores and loose NF membranes with loose selective layers are developed, thus bridging the gap between NF and UF [13].

Up to now, strategies to prepare TUF membranes have been extensively explored, and numerous well-established methods are therefore

* Corresponding author.
** Corresponding author.
*** Corresponding author.
E-mail addresses: xsshi@njtech.edu.cn (X. Shi), xiongsenhg@njtech.edu.cn (S. Xiong), yongwang@njtech.edu.cn (Y. Wang).

https://doi.org/10.1016/j.memsci.2021.119635
Received 8 June 2021; Received in revised form 12 July 2021; Accepted 14 July 2021
Available online 18 July 2021

developed, including phase inversion [14,15], surface modification [16], and interfacial polymerization [17,18]. For example, Ye et al. fabricated TUF membranes through the co-deposition of dopamine (DA) and polyethylenimine (PEI) on hydrolyzed polyacrylonitrile membranes [19]. In our previous study, filling phenolic prepolymers into polyvinylidene fluoride (PVDF) substrates followed by thermal polymerization was also proposed to build TUF membranes with tunable performances [20]. Despite these arresting successes, the further performance improvement of TUF membranes still faces a great challenge, possibly due to the nonuniformity of separation channels and the long, tortuous mass transfer routes. To be specific, the currently available materials to fabricate TUF membranes are mainly amorphous polymers and inorganic ingredients, which inherently impede the uniformity of generated sieving pores [21,22]. Even worse, the tortuous channels are inevitably created, and those TUF membranes would suffer from the permeance-selectivity trade-off originated from the significantly increased transport resistance. Additionally, to maintain satisfying selectivities, thick separation layers are usually required in those TUF membranes, further compromising the separation efficiency [23]. Therefore, there is a pressing need to develop next-generation TUF membranes with ordered channels and thin separation layers.

Covalent organic frameworks (COFs) are a kind of porous and crystalline framework material constructed by covalent bonds, which have shown huge potentials in diverse areas [24]. Since the first report of free-standing COF-based membranes by Banerjee and coworkers in 2017, membranes derived from COFs are continuously developed to fulfill advanced separations, because of the ordered pores and uniform mass transfer routes [25]. Especially for the molecular separation, a number of efforts have been dedicated to shaping COFs into membranes for size-based discrimination [25,26]. At present, some post-modification methods are proposed to satisfy the demand for enhanced separation precision as well, thus achieving the gas and ion separations [27,28]. However, to the best of our knowledge, all of these researches focus on the preparation membranes by microporous COFs, which present aperture sizes in the range of ~0.8–2.5 nm. Thus, they may show decent performances for the purpose of NF, but are barely suitable for the mesopore-required TUF. Fortunately, in light of the reticular chemistry, large-pore COFs (LP-COFs) featuring a mesoporous porosity are synthesized by integrating large building blocks with long linkers [29]. Beyond mesoporous two-dimensional (2D) COFs, a breakthrough in constructing large-pore 3D COFs are also reported by Fang et al. [30] Combined with the attributes of COF-based materials, these LP-COFs have great potentials to build high-performance TUF membranes; however, this still remains to be validated experimentally. We can envision that the dilated channels of LP-COFs are able to effectively repulse the solutes with appropriate sizes, and allow a fast permeation of water. Therefore, together with the highly ordered pores, TUF membranes produced by LP-COFs are likely to display a simultaneously increased water permeance and selectivity.

Herein, for the first time, we introduce the preparation of LP-COF membranes for TUF by a unidirectional diffusion method at room temperature. With the help of this interfacial strategy, continuous and defect-free LP-COF separation layers with a low thickness of only ~60 nm are *in-situ* grown on the top of macroporous substrates. The resultant LP-COF layers as well as their bulk counterparts show desired crystallinity, and a fast infiltration of water into the LP-COF layer is observed. We further systematically analyze the morphological features and surface characteristics of the obtained LP-COF-based TUF membranes. Moreover, the preparation conditions including catalyst location, monomer concentration and reaction time are investigated to optimize the membrane performance. The optimized LP-COF membrane shows exceptional water permeance and high rejections to dye molecules, also, demonstrating a superior dye/salt separation performance.

2. Experimental

2.1. Materials

1,3,5-Tris(*p*-formylphenyl)benzene (TFPB) was purchased from Jilin Chinese Academy of Sciences-Yanshen Technology Co., Ltd. 4,4′-Diaminobiphenyl (BD), 1,4-dioxane, mesitylene, toluene, ethanol and acetic acid were supplied by Aladdin. Methyl orange (MO), chrome black T (EB-T), acid fuchsin (AF), Congo red (CR), Evans blue (EB), and inorganic salts were provided by Sinopharm Chemical Reagent. The CdSe@CdS quantum dots (QDs) dispersed in toluene were obtained from Janus New-Materials. Macroporous polyvinylidene fluoride (PVDF) membranes (diameter: 25 mm, nominal pore size: 0.22 μm, Millipore) were used as the substrates. All reagents were used without further purification. Deionized water (DI water, conductivity: 2–10 μS cm^{-1}) was used in all experiments.

2.2. Seeding treatment of PVDF substrates

2.3 mg of TFPB and 1.7 mg of BD were separately dissolved in 100 mL mesitylene. Subsequently, 10 μL of acetic acid serving as the catalyst was added into the TFPB solution. The obtained mixtures were subjected to the ultrasonic treatment to form homogeneous solutions. To build a seeding layer, PVDF substrates were firstly immersed in the BD solution for 10 min followed by rinsing with mesitylene to remove excessive BD. Next, BD-grafted PVDF substrates were immersed in the TFPB solution for another 10 min, followed by thoroughly washing with mesitylene. In the above procedure, the BD pre-located PVDF substrates can readily react with TFPB to form a seeding layer. To obtain a sufficiently seeded layer, the above procedures were carried out for three times. Then, the seeded PVDF substrates were dried at room temperature for further use. To ensure the successful formation of crystal nuclei, the seeding processes were conducted under a temperature of 10 °C and a humidity of 30%.

2.3. Preparation of LP-COF/PVDF membranes

TFPB (11.7 mg, 0.03 mmol) was dissolved in 40 mL of mesitylene followed by the addition of 1 mL glacial acetic acid. BD (55.3 mg, 0.3 mmol) was dissolved in 40 mL of DI water. A piece of seeded PVDF substrate was then placed between a homemade diffusion cell, and about 10 mL of two monomer solutions were simultaneously injected into the diffusion cell at a constant injection rate using syringes. It should be noted that the aldehyde monomer solution was added into the side facing to the PVDF substrate with the seeding layer. Subsequently, the apparatus was kept undisturbed at room temperature for designed durations. After the reaction, the monomer solutions in both sides were carefully drawn out by a syringe. The resultant LP-COF/PVDF tight ultrafiltration membrane was then taken out and completely cleaned with ethanol and mesitylene. To optimize the separation performance, the addition of acetic acid in water as well as different molar ratios of TFPB/BD were investigated.

2.4. Synthesis of LP-COF powders

LP-COF powders were also synthesized for the structural comparison. Specifically, TFPB (62.5 mg, 0.16 mmol) and BD (44.2 mg, 0.24 mmol) were suspended in a mixture of mesitylene and 1,4-dioxane (1:1 v/v, 6 mL) in a 20 mL glass vial followed by sonication for 10 min to obtain a homogeneous dispersion. Next, acetic acid solution (0.6 mL, 6 M) was slowly added into the mixture. The vial was then left undisturbed at 45 °C for 3 days. The yellow precipitate was collected after thoroughly washing with ethanol and 1,4-dioxane. The product was vacuum dried at 80 °C for 24 h to generate final LP-COF powders.

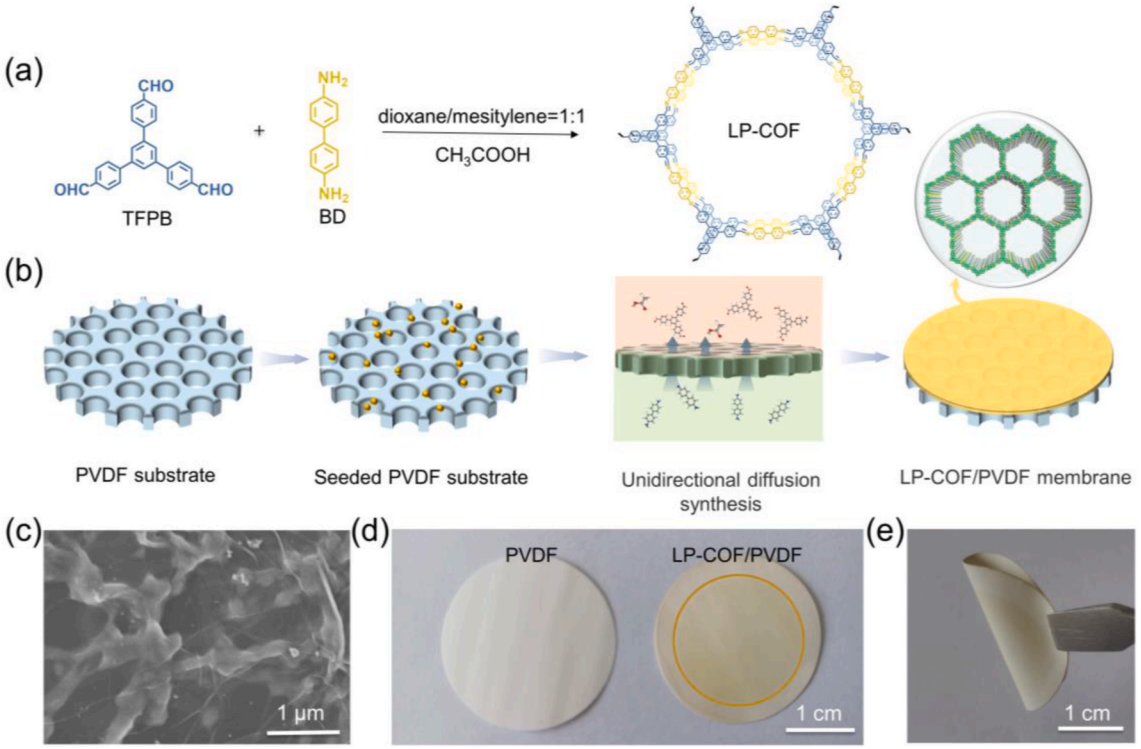

Fig. 1. Preparation of LP-COF/PVDF membranes. (a) Schematic diagram of LP-COF synthesized by the condensation between TFPB and BD. (b) Diagram of the fabrication of the LP-COF membrane by unidirectional diffusion synthesis. (c) Surface SEM image of the LP-COF/PVDF membrane. (d) Photographs of the PVDF substrate, LP-COF/PVDF membrane and (e) the bended LP-COF/PVDF membrane. The LP-COF/PVDF membrane used for characterizations was synthesized for 12 h.

2.5. Characterizations

Fourier transform infrared (FTIR) spectra of the monomers, LP-COF powders and membranes were collected on a Nicolet 8700 spectrometer (Thermo Fisher Scientific) with the wavenumber in the range of 500–4000 cm^{-1}. The membrane samples were measured under the attenuated total reflectance (ATR) mode. X-ray diffraction (XRD) patterns were obtained on a SmartLab X-ray diffractometer (Rigaku Corporation) with the scanning range of 1–30° at a step of 0.02° under room temperature. The morphologies of the LP-COF membranes were observed by a field-emission scanning electron microscope (SEM, S-4800, Hitachi) operating at 5 kV. All samples were in advance ion-sputtered with gold to enhance their conductivity. The ratio of defect areas was evaluated based on the SEM images using a software of Image J. The surface topographies of the membranes were examined by atomic force microscopy (AFM, XE-100, Park Systems), and the scanning rate was 0.5 Hz. The dynamic water contact angle (WCA) measurements were conducted on a contact angle goniometer (Dropmeter A100, Maist). The surface charges of the membranes were analyzed using an electrokinetic analyzer (SurPass, Anton Paar GmbH) with a streaming potential method. 0.1 mmol L^{-1} KCl solution was used as the background electrolyte solution, and the pH values were adjusted by 0.1 mol L^{-1} NaOH and HCl solutions, respectively. The zeta potentials of dyes dispersed in water were obtained by a Zetasizer Nano ZS ZEN3600 electrokinetic analyzer (Malvern, UK).

2.6. Filtration tests

The water permeance and rejection performance of membranes were tested by a dead-end filtration cell (Amicon 8003, Millipore) with an operation pressure of 0.5 bar. Before tests, the membranes were pressurized for at least 10 min to reach a steady state. The water permeance (J_w, L m^{-2} h^{-1} bar^{-1}) was defined by normalizing the volume V (L) of the permeation through the effective area of A (m^2) during the time Δt (h) under the *trans*-membrane pressure P (bar), and calculated by the following equation:

$$J_w = V/(A\ \Delta t\ P) \quad (1)$$

The flux (F, L m^{-2} h^{-1}) during the filtration tests was calculated by the following equation:

$$F = V/(A\ \Delta t) \quad (2)$$

A salt aqueous solution (1000 mg L^{-1}) or a dye aqueous/ethanolic solution (25 mg L^{-1}) was used as the feed solution to evaluate the separation performance. The rejection refers to the percentage of the soluble mass retained by the membrane in the total solute in the solution after filtration. The rejection rate (R, %) was calculated by the following equation:

$$R = (1 - C_p/C_f) \times 100\% \quad (3)$$

where, C_p and C_f are the concentration of permeate and feed solution, respectively. The concentrations of dye molecules and salts in the feed and filtrate were determined by a UV–vis spectrophotometer (Nanodrop 2000c, Thermo Fisher Scientific) and a conductivity meter (S230-K, Mettler-Toledo), respectively.

To perform the separation experiment of QDs, we designed a filtration device, which contained a 5 mL needle tubing and a detachable polypropylene filter with a diameter of 13 mm. The LP-COF/PVDF membrane was then fixed in the middle of the detachable polypropylene filter holders for filtration. 3 mL of QDs dispersion was pre-sucked in a plastic needle tubing serving as the feed, and the filtration process was then carried out by manually pressuring until the complete permeation of the feed. The size distribution of CdSe@CdS QDs was determined by dynamic light scattering (Nanoplus, Micromeritics). Photoluminescence (PL) fluorescent spectra of feed and filtrate were recorded on a Varian Cary Eclipse fluorescence spectrophotometer. The excitation wavelength and voltage were 400 nm and 580 V for toluene

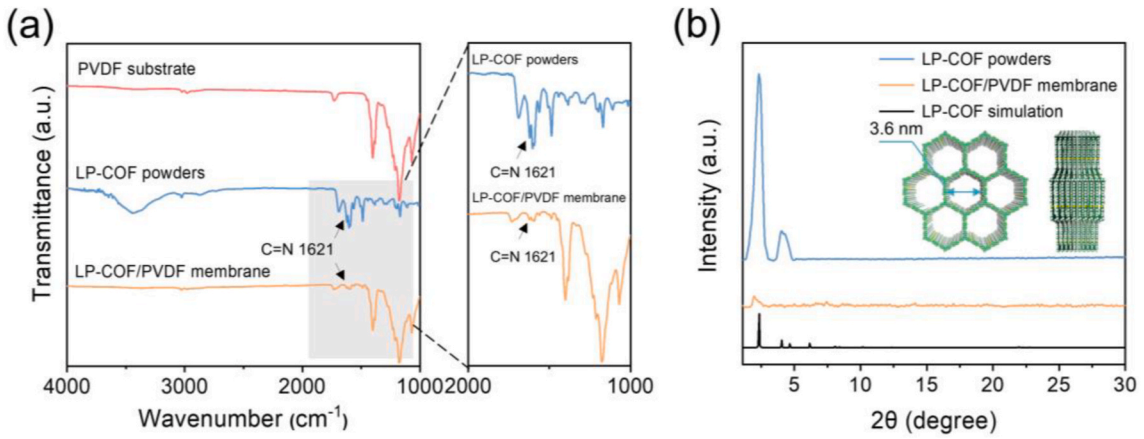

Fig. 2. Structural characterizations. (a) FTIR spectra of the PVDF substrate, LP-COF powders, and LP-COF/PVDF membrane. (b) XRD patterns of the LP-COF powders and LP-COF/PVDF membrane. Insets in (b) is the structural mode of LP-COF with an eclipsed stacked structure. The LP-COF/PVDF membrane used for these characterizations was synthesized for 72 h.

solutions of QDs, respectively.

3. Results and discussion

3.1. Synthesis of LP-COF/PVDF membranes

The synthesis of LP-COF is implemented by the condensation between large aldehyde monomer (TFPB) and long amine linker (BD) *via* Schiff base reaction (Fig. 1a). To maximize the permeance of the synthesized membranes, PVDF substrate with a nominal pore size of up to ~0.22 μm was chosen as the support to grow LP-COF layer. In this work, the LP-COF membranes were prepared by the unidirectional diffusion method reported in our previous work (Fig. 1b) [31]. Specifically, the aldehyde organic solution and amine aqueous solution were separately loaded at the two sides of the seeded PVDF substrate to give an organic-water interface (Fig. S1). Due to the good affinity between the amines and organic solvent, amine molecules tend to diffuse into the organic phase upon the formation of the interface. When the amines contact with aldehydes, the polymerization between them happens at the interface with the assistance of catalyst, thus generating a thin and continuous LP-COF layer on the PVDF substrate. It should be noted that the use of bare PVDF substrates produces LP-COF layers with noticeable defects under a prolonged duration (Fig. S2), and this can be rationalized due to the large pore size and relatively inert surface of substrates. In order to solve this issue, the seeding procedure is introduced to form massive crystallites on the PVDF substrate (Fig. S3). During the interfacial polymerization, these crystallites can serve as the nucleation sites to facilitate the growth of LP-COF, which has been extensively clarified by previous studies [32,33]. With the aid of these crystallites, a defect-free LP-COF layer can be easily formed within 12 h (Fig. 1c). The generation of the LP-COF layer is also supported by the appearance variation of substrates, whose color changes from white to buff (Fig. 1d). Thanks to the flexible polymer support and pure organic network of LP-COF, thus-synthesized LP-COF membranes display a good flexibility, which can be repeatedly bended without noticeable breakages (Fig. 1e).

The formation of LP-COF separation layer on PVDF substrate was

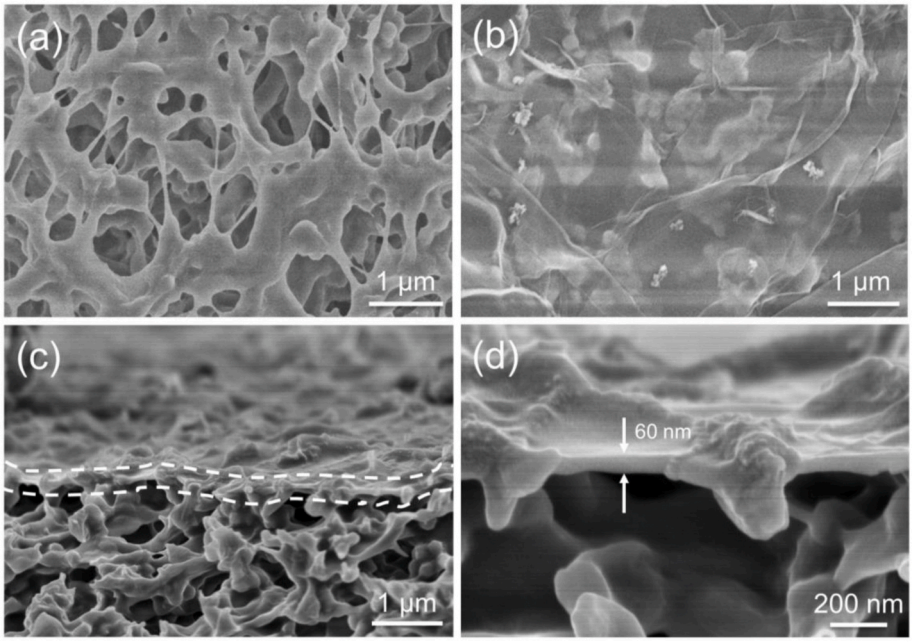

Fig. 3. Morphologies of the different membranes. (a) Surface SEM image of the PVDF substrate. (b) Surface and (c, d) cross-sectional SEM images of the LP-COF/PVDF membrane synthesized for 12 h.

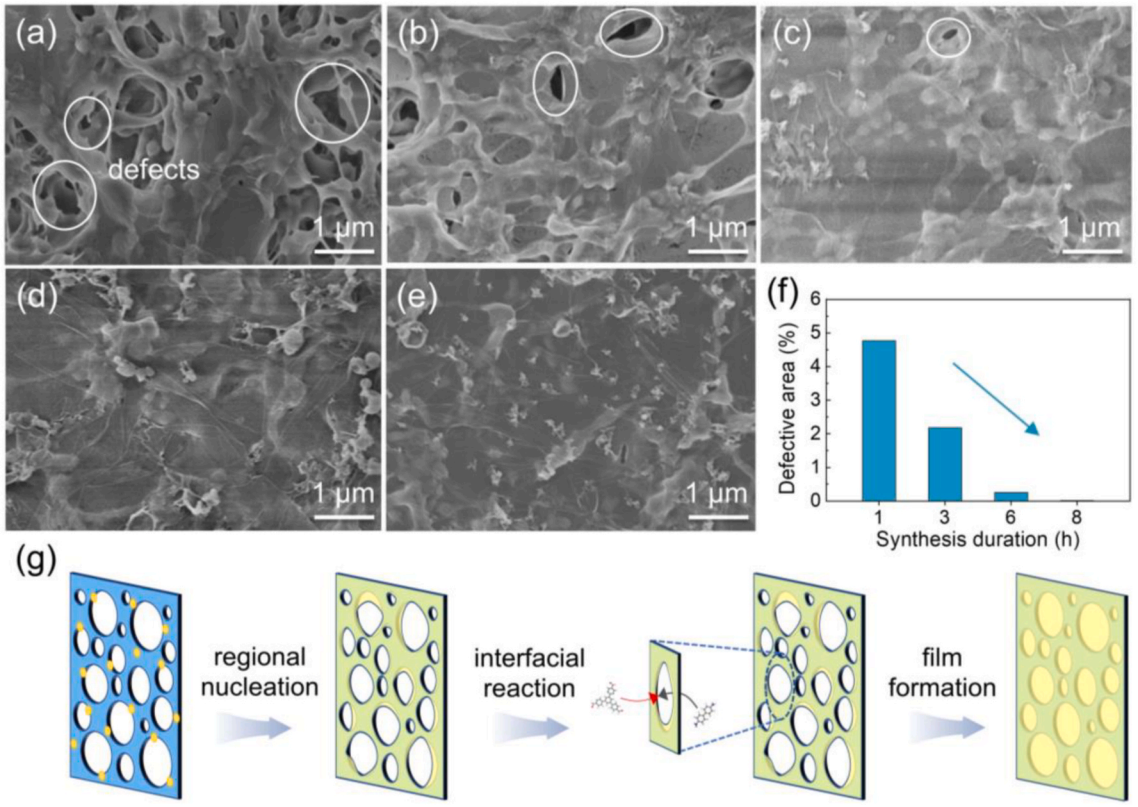

Fig. 4. Formation of the LP-COF/PVDF membranes. Surface SEM images of the LP-COF/PVDF membranes synthesized for (a) 1 h, (b) 3 h, (c) 6 h, (d) 8 h, (e) 10 h. (f) Ratio of the defective area to the total area as a function of the growth time. (g) Diagram for the formation of the LP-COF/PVDF membrane.

confirmed by FTIR analysis. Comparing the spectrum of the LP-COF/PVDF membrane with that of monomers (Figs. 2a and S4), the stretching vibration peak of CH═O (1687 cm^{-1}) originated from TFPB is largely weakened. Meanwhile, the N–H stretching vibration peaks of BD at 3203, 3321, and 3386 cm^{-1} basically disappear. These results indicate the sufficient consumption of monomer pairs. Moreover, after the condensation reaction, the characteristic peak of C═N stretching vibration (1621 cm^{-1}) appears in the spectrum of the membrane. The emergence of new peaks and the disappearance of peaks corresponding to monomers are also observed in the spectrum of LP-COF powders, which is in consistence with the results previously reported in literature [34,35]. Thus, results of these FTIR spectra prove the generation of imine linkages to give a LP-COF layer on the substrate. The crystallinity of the formed LP-COF layers was further determined by XRD measurement. As can be seen from Fig. 2b, the XRD pattern of the membrane shows a noticeable diffraction peak at ~2.0°, consistent with the 2 theta value observed from the patterns of the LP-COF powders and simulated result. This indicates a similar structure for LP-COF generated by the solvothermal synthesis and unidirectional diffusion method. Specifically, the peak at ~2.0° can be assigned to the (100) crystal plane, and the produced LP-COF correspondingly presents an AA stacking mode with an aperture size of up to ~3.6 nm [34], as illustrated in Fig. 2b. It should be noted that, the attenuation in the peak intensity of the LP-COF membrane is mostly caused by the extremely low thickness of the LP-COF layer shown below [36]. Also, the preparation under ambient conditions could possibly give rise to the weakening of crystallinity. Considering the balance between the crystallinity of COF layers and the complexity of the preparation comprehensively, we believe that synthesizing the LP-COF membranes through this strategy still hold advantages compared with other COF membranes produced under extreme conditions [37].

3.2. Microstructures of LP-COF/PVDF membranes

SEM observations were carried out to reveal the surface and cross-sectional morphologies of as-synthesized membranes. As shown in Figs. 3a and S5, the pristine PVDF substrate presents a cave-like structure scattered with many macropores. After synthesizing for 12 h, the macroporous PVDF substrate is completely covered with a continuous LP-COF layer (Fig. 3b). The obtained LP-COF layer is in absence of any cracks, pinholes, or defects, and displays a wrinkly topography (Fig. S6). Moreover, through the LP-COF layer we can faintly observe the macropores of underneath PVDF substrates, implying a low thickness of the top LP-COF layer. The cross-sectional morphology of the obtained membrane is thereby disclosed with the result given in Fig. 3c. Obviously, it shows that the LP-COF layer is well intergrown with the substrate in the absence of any gaps, indicative of a good adhesion between these two layers. This intergrowth benefits from the construction of the seeding layer, which ensures the *in-situ* nucleation growth of LP-COF on the substrate [38]. Further, the enlarged cross section exposes the reduced thickness of the LP-COF layer, which is about 60 nm (Fig. 3d). Besides, the LP-COF layer is exclusively located on the top surface (Figs. S7 and S8), indicating that the permeability of the macroporous substrate is excellently preserved. This will in return enable an increased permeance for the fabricated composite membrane [39].

3.3. Formation of LP-COF/PVDF membranes

To investigate the formation mechanism of the continuous LP-COF layer, we prepared a series of LP-COF membranes under various synthesis durations. As shown in Fig. 4a–e, the LP-COF layer undergoes a repairing process, in which the defect area is continuously reduced to give a dense surface. To be specific, the short synthesis duration of 1 h generates the membrane with obvious micron-sized discontinuous defects (Fig. 4a). With an extended duration of 3 h, the defective area is

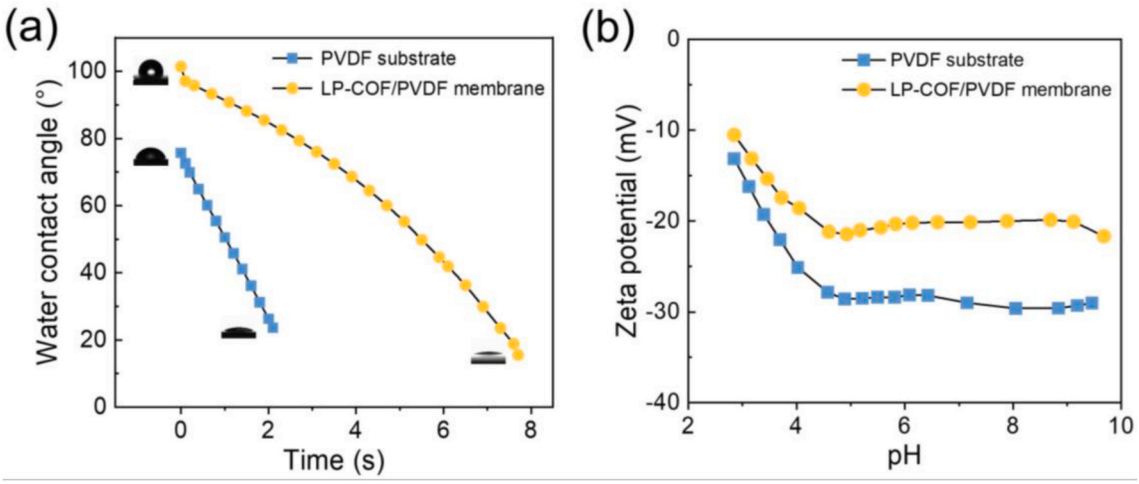

Fig. 5. Surface properties of different membranes. (a) Dynamic water contact angles and (b) Zeta potentials of the PVDF substrate and LP-COF/PVDF membrane. Insets in (a) are photographs showing the initial and final water contact angle.

distinctly decreased (Fig. 4b). Subsequently, we can obtain a defect-free LP-COF layer with a duration of 8 h (Fig. 4d). The ratio of the defective area to the total area versus the synthesis duration is depicted in Figs. 4f and S9. Consistent with the SEM observations, the value sharply decreases with the synthesis duration, reaching nearly zero at 8 h. On the basis of above results, the formation of continuous LP-COF layers is probably promoted by the combination of the regional nucleation and interfacial reaction, as illustrated in Fig. 4g. Initially, the seeding preformed on the skeleton of PVDF substrates acts as the nucleation site to induce the regional nucleation. This starts the lateral growth of LP-COF to bring about a covering layer on the PVDF skeleton. Meanwhile, the formed LP-COF coverage may slightly extend to the porous

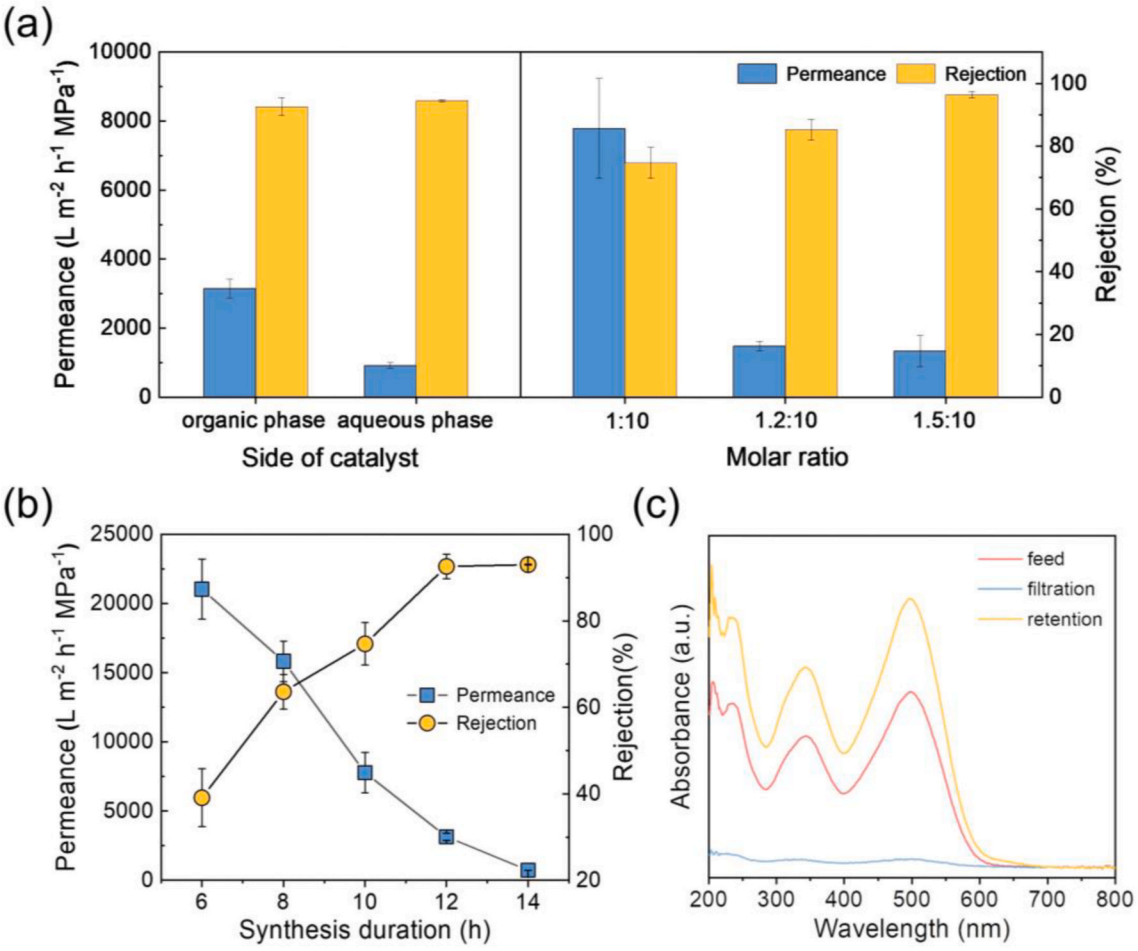

Fig. 6. Performance optimization of the LP-COF/PVDF membrane. (a) Influence of the location of catalyst, molar ratio, and (b) synthesis durations on the performances. (c) UV–vis absorption spectra of the feed, filtration, and retention obtained by rejecting CR.

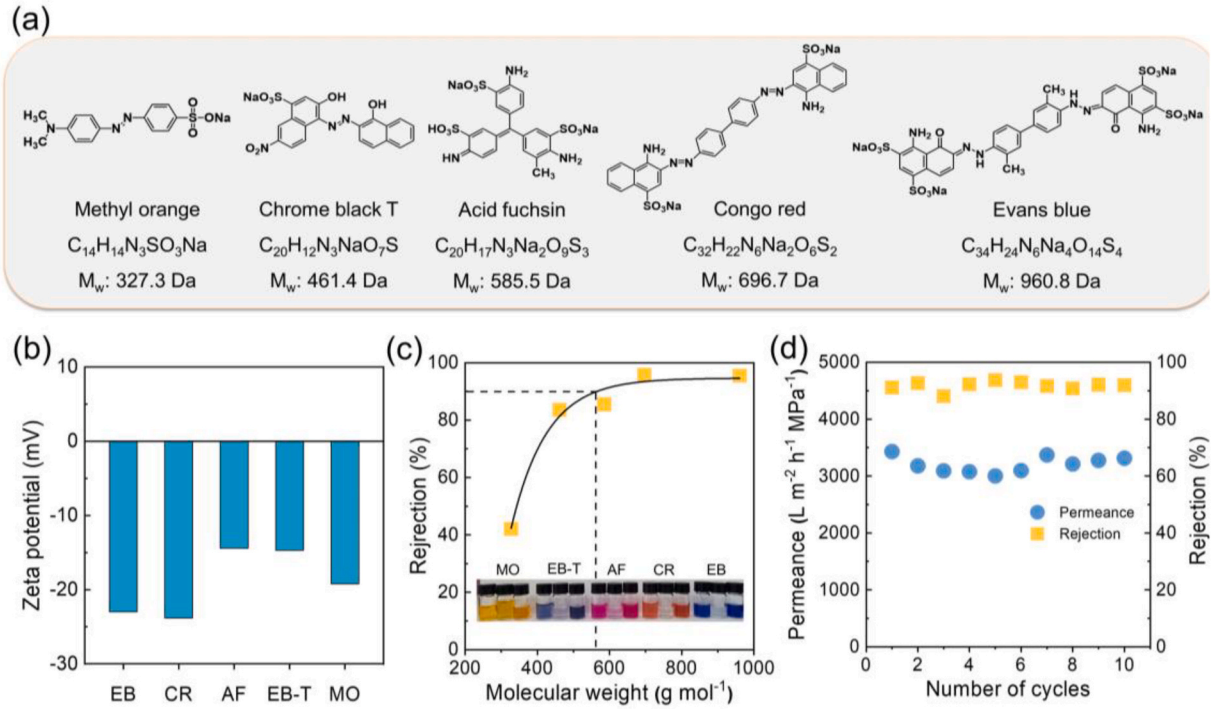

Fig. 7. Separation performance of the optimized LP-COF/PVDF membrane. (a) Structures and (b) zeta potentials of the used dye molecules. (c) Rejections to different dye molecules. (d) Stability in terms of number of cycles. Insets in (c) are photographs showing the color change of various dye solutions including feed, filtration, and retention.

area of substrates. However, due to the large size of these pores, a full cover can be hardly realized by LP-COF generated by the local nucleation. Then, the interfacial reaction between monomers accounts for the growth of LP-COF at the unblocked area, ensuring the successive growth of the LP-COF layer. It must be noted that the interfacial reaction prefers to occur at the defective location, as it allows a free diffusion of amines from water to the organic phase, and thus eliminates the existing gaps to form a defect-free, continuous LP-COF layer. Upon the generation of a complete LP-COF layer, the penetration of monomers is greatly hampered because of the increased mass transfer resistance, leading to a self-limited growth of the LP-COF layer to give a reduced thickness (Fig. S10).

3.4. Surface properties of LP-COF/PVDF membranes

Fig. 5a shows the dynamic WCAs of the bare PVDF substrate and LP-COF membrane. With the coverage of a continuous LP-COF layer, the preliminary WCA is increased from ~75.7° to ~101.4°, signifying a relatively hydrophobic surface. This is mainly due to the hydrophobic aromatic skeleton of the formed LP-COF. Although the hydrophobicity is involved, the water droplet rapidly penetrates into the LP-COF membrane with a short duration of only ~8 s, benefiting from the large-pore structure which allows an unobstructed infiltration of water. The macroporous substrate underneath the LP-COF layer may contribute to the water penetration as well. This collectively accelerated water penetration will facilitate the permeation of water during filtration, which is favorable for the promotion of water permeance [39]. Further, the Zeta potential analysis reveals a negatively charged surface of the LP-COF membrane at the tested pH value of ~3–10 (Fig. 5b).

3.5. Performance optimization of LP-COF/PVDF membranes

Ordered mesoporous channels of the LP-COF layer can work as the high-efficiency mass transfer paths to allow the fast transport of solvent, while rejecting large-sized solutes based on the size sieving. Additionally, the negatively charged surface of the membrane endows the electrostatic repulsion to the molecules with the same charge, contributing to the improvement of rejection rate. Considering the synergy offered by the LP-COF membrane, it is likely that the high water permeance and high selectivity can be simultaneously obtained [40]. We then optimized the preparation conditions, and CR (M_w = 696.8 Da, size = 2.56 × 0.73 × 1.13 nm^3) dispersed in water was used to evaluate the performance of the membranes synthesized under various parameters. In view of the different diffusion rate of acetic acid in organic and water bulk phase [41], the influence of the catalyst location was first investigated with results given in Fig. 6a. It can be seen that the produced membranes exhibit similar CR rejection rates under a constant synthesis duration of 12 h. Nevertheless, the permeance obtained by loading catalyst in the organic phase is 3-fold higher than the result generated by the other condition. To clarify this difference, we checked the morphologies of these two types of membranes. Clearly, the membrane prepared by loading the catalyst in water shows a massif-like structure (Fig. S11), which undoubtedly rises the mass transfer resistance to decrease the water permeance. In the following investigation, the load of the acetic acid was thus fixed in the organic side. The monomer amount certainly determines the reaction speed and the thickness of the obtained films, we thereby studied its influence on the membrane performance. Notably, the molar ratio of TFPB/BD was varied from 0.8:10 to 1.5:10, but the molar ratio of 0.8:10 generated the membrane having a discontinuous LP-COF layer (Fig. S12). For that reason, the performance of the membranes prepared with a molar ratio ranging from 1:10 to 1.5:10 was tested. As shown in Fig. 6a, these LP-COF membranes consistently give a high rejection rate to CR, while the permeance significantly decreases with the rise of the molar ratio, which is caused by the increasingly raised thickness of the LP-COF layer (Fig. S13). In particular, the LP-COF membrane synthesized with the molar ratio of 1.5:10 gives a water permeance of ~1333 L m^{-2} h^{-1} MPa^{-1}, which is only ~17.1% of the value obtained under 1:10. Therefore, the molar ratio of 1:10 will be utilized as the synthesis parameter for the next investigation.

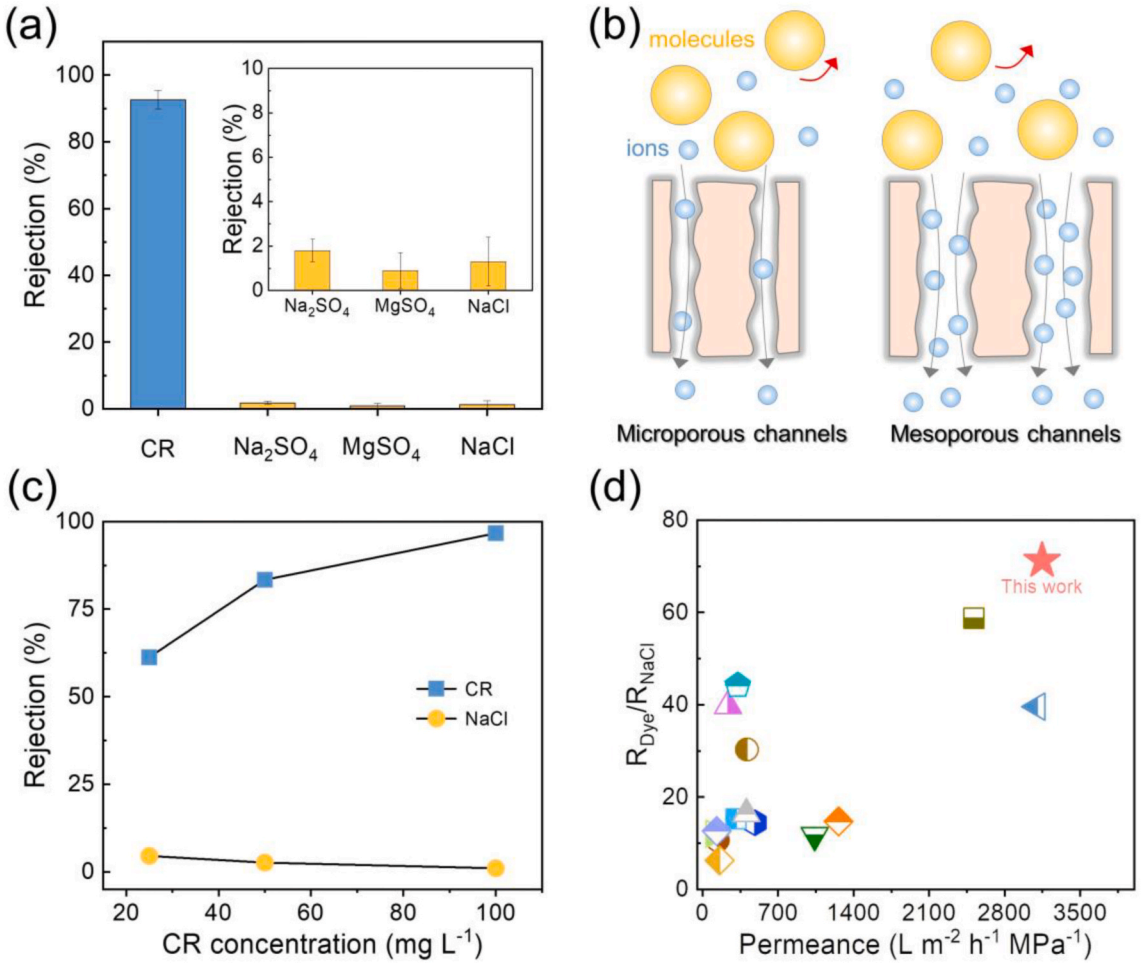

Fig. 8. Dye/salt separation performance of the optimized LP-COF/PVDF membrane. (a) Rejection to various inorganic salts. (b) Schematic diagram of the dye/salt separation by size-varied pores. (c) Rejection to CR and NaCl under different CR concentrations. (d) Comparison on the dye/salt separation performance.

Apart from the two conditions studied above, we also checked the influence of the duration on the membrane performance. Fig. 6b visibly reveals that the variation tendencies of the permeance and rejection are opposite with the duration increasing from 6 to 12 h. For instance, the LP-COF membrane synthesized for 8 h shows an extremely high permeance of up to ~15,832 L m^{-2} h^{-1} MPa^{-1} with a moderate CR rejection of ~63.6%. It should be noted that the water permeance of the bare PVDF substrate is ~47,580 L m^{-2} h^{-1} MPa^{-1}, which gives negligible rejections (<5%) to dyes (Fig. S14). Thus, the coverage of a continuous LP-COF layer effectively promotes the selectivity in the presence of an acceptable sacrifice in permeance. The extension on the synthesis duration benefits the elimination of the possibly existed intercrystalline defects. Besides, the stack of LP-COF films at the wrinkle area may result in interlaced pores to decrease the effective sieving pore size, thus promoting the selectivity to some degree [42,46]. As expected, the membrane synthesized for 12 h achieves a pronounced CR rejection of ~92.6%, and the water permeance is still as high as ~3147 L m^{-2} h^{-1} MPa^{-1}. It is noteworthy that the performance displayed by our LP-COF membranes outperforms the vast majority of microporous COF-based membranes for dye separations (Fig. S15 and Table S1) [43]. Further prolonging the synthesis duration to 14 h produces a continuous decrease in water permeance as well as a constant rejection rate. Hence, given the balance between the permeance and selectivity, the optimized synthesis duration is believed to be 12 h, which gives a maximized separation performance. One may argue that the pronounced rejection may be caused by the adsorption of CR on the membrane. We accordingly checked the concentration of CR in the retentate. As shown in Fig. 6c, the UV–vis absorption spectra signifies a noticeable increase in the CR concentration of retentate, eliminating the above-mentioned concern [31].

3.6. Separation performance of the optimized LP-COF/PVDF membrane

A series of dyes with different molecular weights were then used as the probe molecule to systematically evaluate the separation performance of the optimized LP-COF/PVDF membrane. Fig. 7a presents the detailed molecular structures of the corresponding dyes, which are all negatively charged with Zeta potential ranging from ~-15 to ~ -24 mV (Fig. 7b). The rejection curve of the membrane toward those dyes is shown in Fig. 7c. Observably, increasing the molecular weight of dyes brings about an improved rejection rate, which reaches ~95.5% and ~95.8% for EB and CR, respectively. The dye concentrations in the retentates are also increased (Fig. S16), indicative of the absence of the adsorption. The deepened color of the retentate solutions further verifies this (inset in Fig. 7c). To gain insights into the separation mechanism, we tested the rejections of dyes dispersed in ethanol, in which the electrostatic repulsion is greatly shielded [44,45]. Fig. S17 shows that the rejection rates in ethanol are visibly decreased, but still keep at a moderate level instead of an extremely low level. Thus, the result suggests that the prominent separation performance is mostly ascribed to the synergy of size exclusion and electrostatic repulsion. Moreover, different from the other studies which report a dye rejection exceeding 99%, the rejection observed in this work is slightly reduced because of the enlarged pore size. It is noteworthy that, compared to the pure water

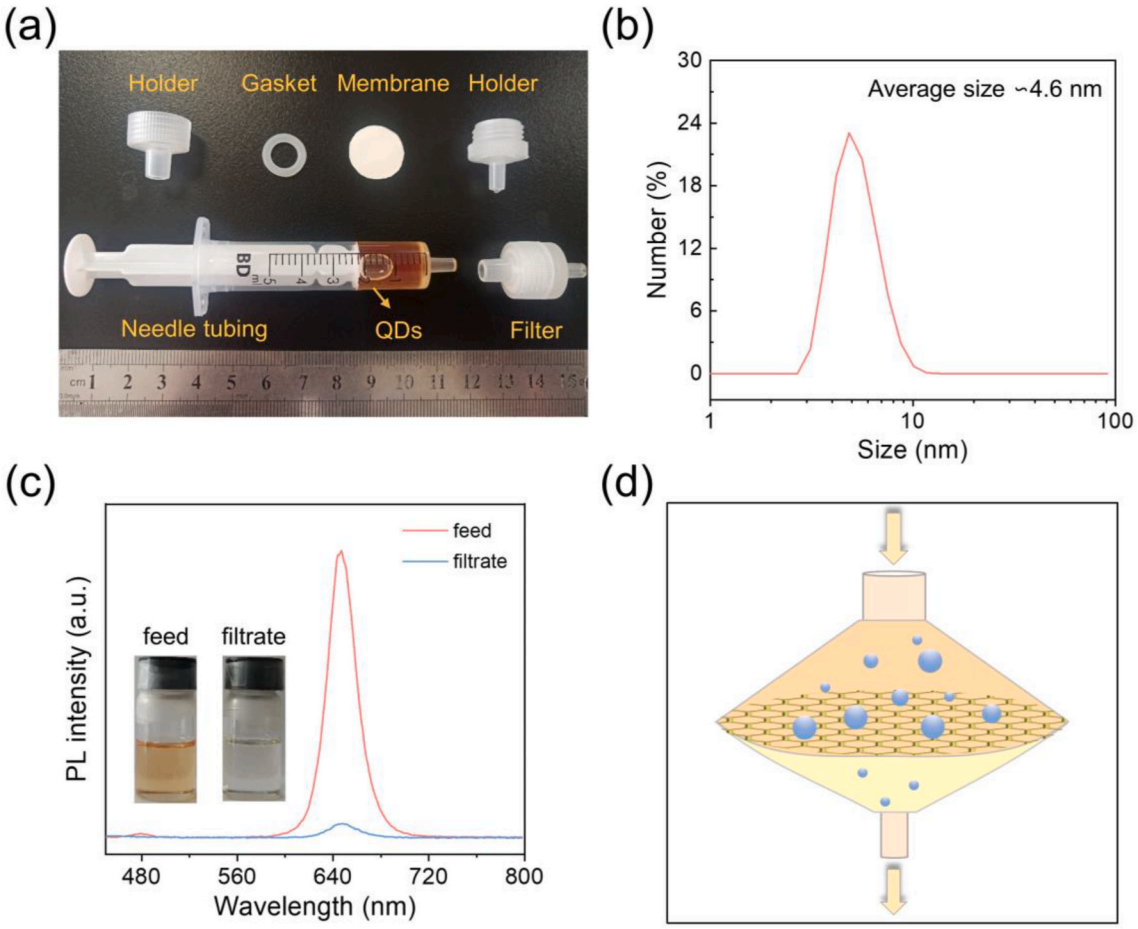

Fig. 9. Separation of QDs in toluene by the optimized LP-COF/PVDF membrane. (a) All parts of the dismountable filter holder. (b) Particle size distribution of the original QDs dispersion. (c) Fluorescent spectra of QDs in the feed and filtrate, and the insets are the corresponding optical photographs under sunlight. (d) Schematic illustration of the separation.

flux, the permeation fluxes of dye solutions during filtration tests are largely retained (Fig. S18), indicating the practicability of our membranes. Intriguingly, considering the high selectivity and high permeance, the LP-COF membrane exhibits a remarkable processing capability as well as an acceptable separation efficiency, which far exceeds the performance of other works summarized in Table S2. In additional, the rejection curve generates a dye molecular weight cut-off (MWCO) of ~560 Da for the LP-COF membrane. The obtained dye MWCO is comparable to that of the membranes constructed by microporous COFs. Taking TpPa and COF-LZU1 as the examples, their membranes display a dye MWCO of ~600 and ~450 Da, respectively [31,46]. The reusability of the LP-COF membrane was evaluated by discontinuously filtrating for several cycles. After each cycle, the dyes concentrated on the membrane surface can be readily cleaned by simply ethanol washing (Fig. S19). Furthermore, the permeance and CR rejection rate are basically unchanged after 10 cycles of use (Figs. 7d and S20). These results not only confirm an excellent reusability, but also indicate a superior adhesion between the LP-COF separation layer and PVDF substrate. After soaking the LP-COF membrane in water for several days, inappreciable changes in the separation performance are observed (Fig. S21), stating its favorable water stability. Therefore, the LP-COF membrane produced by the *in-situ* interfacial strategy may satisfy the need of practical application, ensuring a desired stability in the aspect of both structure and performance.

3.7. Dye/salt separation performance

Given the inherent mesopores of the LP-COF membrane, they may benefit an accelerated permeation of small solutes with a size blow 1 nm. Together with the high removal efficiency of dye molecules presented above, we anticipate that thus-synthesized LP-COF membranes could work as a powerful platform for the separation of dye/salt mixture. To confirm this, the rejections of the optimized LP-COF membranes toward different inorganic salts were tested, with the result given in Fig. 8a. It can be seen that, the membrane keeps a desired CR rejection as high as ~92.6%, while it delivers extremely low rejections to ions. For example, the rejections to Na_2SO_4, $MgSO_4$, and NaCl are ~1.8%, ~0.9% and ~1.3%, respectively. Meanwhile, the low rejection rates are observed for salts with varied concentrations (Fig. S22). Impressively, the salt rejections are even lower than those of the membranes designed for dye/salt separation [47,48], profiting from the broadened channels (Fig. 8b). To further confirm the feasibility of LP-COF membranes for high-performance dye/salt separation, the filtration tests were conducted by using the mixture comprising of 1000 ppm NaCl and concentration-varied CR aqueous solution. As shown in Fig. 8c, the rejections to NaCl still keep at a quite low level under different CR concentrations. The decreased CR rejection under a low CR concentration can be mostly due to the adsorption of Na^+ on the negatively charged surface, which impairs the electrostatic repulsion to slightly allow the pass of CR [49]. Under a CR concentration of 100 ppm, the membrane shows a high rejection (~96.7%) to CR and a very low rejection (~1.0%) to NaCl, which evidently displays a prominent selectivity between ions and dyes. To highlight this dye/salt separation efficiency, the ratio of the rejection rates for dye and NaCl (R_{Dye}/R_{NaCl}) obtained by our membranes was then compared with that of the state-of-the-art membranes (the detailed information is given in Table S3). As shown in Fig. 8d, the

LP-COF/PVDF membrane exhibits a simultaneously improved water permeance and R_{Dye}/R_{NaCl} value, surpassing most of recently reported membranes engineered for dye/salt separation.

3.8. Size-exclusion of QDs in toluene

The resultant LP-COF membranes have demonstrated a favorable molecular separation performance. In conjunction with the solvent resistance, they may be applicable in the extraction of nanoparticles from aggressive solvents. As a proof-of-concept, the optimized LP-COF membrane was used to concentrate nano-sized QDs dispersed in toluene, imminently desired in the field of sensing [50]. The test was performed using a home-made filtration device, in which the membrane was first assembled into a filter shown in Fig. 9a. The dynamic light scattering analysis recognizes that the diameter of QDs is in the range of ~3.1–11.7 nm, giving an average diameter of ~4.6 nm (Fig. 9b). As shown in Fig. 9c, the fluorescence spectrum of the original QDs dispersion shows a strong peak centered at the wavelength of ~647 nm. In contrast, the peak intensity of the permeation collected after the membrane filtration is significantly reduced, matching well with the color change (inset in Fig. 9c). These results evidence the effective rejection of QDs. We reason that the weak peak appeared in the filtrate may be caused by the penetration of small-sized QDs, which could pass through the LP-COF membrane with a negligible rejection (Fig. 9d). In short, the LP-COF membrane realizes the recovery of QDs from toluene, and its application in extracting valuable nanoparticles from organic solvents is expected.

4. Conclusions

In conclusion, benefiting from the unique mesopores of LP-COF, we have successfully prepared highly permeable TUF membranes for ultra-fast separations. The combination of the partial nucleation at the seeded sites and the interfacial polymerization promotes the formation of continuous LP-COF layers. By tuning the synthesis conditions including the molar ratio of monomers, catalyst location, and synthesis duration, the optimized LP-COF layer with a thickness of ~60 nm is formed on the PVDF substrate. Thanks to the ordered mesopores and low thicknesses, the resulting membrane demonstrates a remarkable, stable molecular separation performance, showing an ultra-high water permeance of ~3147 L m^{-2} h^{-1} MPa^{-1} and a favorable CR rejection of ~92.6%. Moreover, very low rejections (<2%) to a series of inorganic salts are observed for the membrane, and then it empowers an outstanding dye/salt separation performance which is ~2–10 times higher than other state-of-the-art membranes. The membrane also demonstrates potentials to recover nanoparticles from organic solvents due to the good solvent resistance of both LP-COF and PVDF substrates. Overall, we expect this work to guide the design of high-performance TUF membranes, and encourage the further exploration of large-pore COFs.

CRediT authorship contribution statement

Siyu Fang: Investigation, Methodology, Writing – original draft. **Xiansong Shi:** Investigation, Writing – review & editing, Funding acquisition. **Xingyuan Wang:** Investigation. **Zhe Zhang:** Investigation. **Congcong Yin:** Investigation. **Zhipeng Zhang:** Investigation. **Tong Ju:** Investigation. **Sen Xiong:** Investigation, Funding acquisition. **Yong Wang:** Supervision, Writing – review & editing, Funding acquisition.

Declaration of competing interest

The authors declare that they have no known competing financial interests or personal relationships that could have appeared to influence the work reported in this paper.

Acknowledgements

Financial supports from the National Science Foundation of China (21908096), the Jiangsu Natural Science Foundation (BK20190677), and the China Postdoctoral Science Foundation (2020M681568) are acknowledged.

Appendix A. Supplementary data

Supplementary data to this article can be found online at https://doi.org/10.1016/j.memsci.2021.119635.

References

[1] S. Zhang, S. Zhao, X. Jing, Z. Niu, X. Feng, Covalent organic framework-based membranes for liquid separation, Org. Chem. Front. 8 (2021) 3943–3967.
[2] E. Santigosa-Murillo, S. Maspoch, M. Munoz, M. Ramos-Payan, An efficient microfluidic device based on electromembrane extraction for the simultaneous extraction of acidic and basic drugs, Anal. Chim. Acta 1160 (2021), 338448.
[3] B. Moyo, M. Gitari, N.T. Tavengwa, Application of sorptive micro-extraction techniques for the pre-concentration of antibiotic drug residues from food samples - a review, Food Addit. Contam. Part A-Chem. 37 (2020) 1865–1880.
[4] C.R. Holkar, A.J. Jadhav, D.V. Pinjari, N.M. Mahamuni, A.B. Pandit, A critical review on textile wastewater treatments: possible approaches, J. Environ. Manag. 182 (2016) 351–366.
[5] X. Li, S. Shen, Y. Xu, T. Guo, H. Dai, X. Lu, Application of membrane separation processes in phosphorus recovery: a review, Sci. Total Environ. 767 (2021) 144346.
[6] Y.-l. Liu, Y.-y. Zhao, X.-m. Wang, X.-h. Wen, X. Huang, Y.F. Xie, Effect of varying piperazine concentration and post-modification on prepared nanofiltration membranes in selectively rejecting organic micropollutants and salts, J. Membr. Sci. 582 (2019) 274–283.
[7] S. Bano, A. Mahmood, S.-J. Kim, K.-H. Lee, Graphene oxide modified polyamide nanofiltration membrane with improved flux and antifouling properties, J. Mater. Chem. 3 (2015) 2065–2071.
[8] Z. Wang, Z. Wang, S. Lin, H. Jin, S. Gao, Y. Zhu, J. Jin, Nanoparticle-templated nanofiltration membranes for ultrahigh performance desalination, Nat. Commun. 9 (2018) 2004.
[9] Z. Tan, S. Chen, X. Peng, L. Zhang, C. Gao, Polyamide membranes with nanoscale turing structures for water purification, Science 360 (2018) 518–521.
[10] X. Shi, A. Xiao, C. Zhang, Y. Wang, Growing covalent organic frameworks on porous substrates for molecule-sieving membranes with pores tunable from ultra- to nanofiltration, J. Membr. Sci. 576 (2019) 116–122.
[11] C. Zhang, J. Zhou, X. Ye, Z. Li, Y. Wang, Zwitterionization of tertiary amines in nanoporous block copolymers: toward fouling-resistant ultrafiltration membranes, Macromolecules 54 (2021) 4236–4245.
[12] J. Wang, Y. Liu, T. Liu, X. Xu, Y. Hu, Improving the perm-selectivity and anti-fouling property of UF membrane through the micro-phase separation of PSf-b-PEG block copolymers, J. Membr. Sci. 599 (2020) 117851.
[13] J. Lin, W. Ye, M.-C. Baltaru, Y.P. Tang, N.J. Bernstein, P. Gao, S. Balta, M. Vlad, A. Volodin, A. Sotto, P. Luis, A.L. Zydney, B. Van der Bruggen, Tight ultrafiltration membranes for enhanced separation of dyes and Na_2SO4 during textile wastewater treatment, J. Membr. Sci. 514 (2016) 217–228.
[14] C. Liu, H. Mao, J. Zheng, S. Zhang, In situ surface crosslinked tight ultrafiltration membrane prepared by one-step chemical reaction-involved phase inversion process between activated PAEK-COOH and PEI, J. Membr. Sci. 538 (2017) 58–67.
[15] G. Han, Y. Feng, T.S. Chung, M. Weber, C. Maletzko, Phase inversion directly induced tight ultrafiltration (UF) hollow fiber membranes for effective removal of textile dyes, Environ. Sci. Technol. 51 (2017) 14254–14261.
[16] D. Zou, X. Chen, M. Qiu, E. Drioli, Y. Fan, Flux-enhanced α-alumina tight ultrafiltration membranes for effective treatment of dye/salt wastewater at high temperatures, Separ. Purif. Technol. 215 (2019) 143–154.
[17] J.M. Tesha, D.S. Dlamini, S. Qaseem, Z. Cui, J. Li, Tight ultrafiltration: layer deposition of trimesoyl chloride/β-cyclodextrin onto polysulfone/poly (styrene-co-maleic anhydride) membrane for water treatment, J. Environ. Chem. Eng. 8 (2020) 103733.
[18] D. Kang, H. Shao, G. Chen, X. Dong, S. Qin, Fabrication of highly permeable PVDF loose nanofiltration composite membranes for the effective separation of dye/salt mixtures, J. Membr. Sci. 621 (2021) 118951.
[19] W. Ye, K. Ye, F. Lin, H. Liu, M. Jiang, J. Wang, R. Liu, J. Lin, Enhanced fractionation of dye/salt mixtures by tight ultrafiltration membranes via fast bio-inspired co-deposition for sustainable textile wastewater management, Chem. Eng. J. 379 (2020) 122321.
[20] Q. Lan, Z. Wang, Y. Wang, Mesoporous phenolics filled in macroporous membranes for tunable tight-ultrafiltration, Chem. Eng. Sci. 187 (2018) 98–106.
[21] S. Zhao, Z. Wang, A loose nano-filtration membrane prepared by coating HPAN UF membrane with modified PEI for dye reuse and desalination, J. Membr. Sci. 524 (2017) 214–224.
[22] Q. Zhang, L. Fan, Z. Yang, R. Zhang, Y.-n. Liu, M. He, Y. Su, Z. Jiang, Loose nanofiltration membrane for dye/salt separation through interfacial polymerization with in-situ generated TiO_2 nanoparticles, Appl. Surf. Sci. 410 (2017) 494–504.

[23] H. Qin, W. Guo, P. Gao, H. Xiao, Customization of ZrO_2 loose/tight bilayer ultrafiltration membranes by reverse micelles-mediated aqueous sol-gel process for wastewater treatment, J. Eur. Ceram. Soc. 41 (2021) 2724–2733.
[24] K. Geng, T. He, R. Liu, S. Dalapati, K.T. Tan, Z. Li, S. Tao, Y. Gong, Q. Jiang, D. Jiang, Covalent organic frameworks: design, synthesis, and functions, Chem. Rev. 120 (2020) 8814–8933.
[25] S. Kandambeth, B.P. Biswal, H.D. Chaudhari, K.C. Rout, H.S. Kunjattu, S. Mitra, S. Karak, A. Das, R. Mukherjee, U.K. Kharul, R. Banerjee, Selective molecular sieving in self-standing porous covalent-organic-framework membranes, Adv. Mater. 29 (2017) 1603945.
[26] M. Matsumoto, L. Valentino, G.M. Stiehl, H.B. Balch, A.R. Corcos, F. Wang, D. C. Ralph, B.J. Mariñas, W.R. Dichtel, Lewis-acid-catalyzed interfacial polymerization of covalent organic framework films, Chem 4 (2018) 308–317.
[27] C. Liu, Y. Jiang, A. Nalaparaju, J. Jiang, A. Huang, Post-synthesis of a covalent organic framework nanofiltration membrane for highly efficient water treatment, J. Mater. Chem. 7 (2019) 24205–24210.
[28] R. Zhao, H. Wu, L. Yang, Y. Ren, Y. Liu, Z. Qu, Y. Wu, L. Cao, Z. Chen, Z. Jiang, Modification of covalent organic frameworks with dual functions ionic liquids for membrane-based biogas upgrading, J. Membr. Sci. 600 (2020) 117841.
[29] L. Wang, Y. Xie, Y. Yang, H. Liang, L. Wang, Y. Song, Electroactive covalent organic frameworks/carbon nanotubes composites for electrochemical sensing, ACS Appl. Nano Mater. 3 (2020) 1412–1419.
[30] Y. Wang, Y. Liu, H. Li, X. Guan, M. Xue, Y. Yan, V. Valtchev, S. Qiu, Q. Fang, Three-dimensional mesoporous covalent organic frameworks through steric hindrance engineering, J. Am. Chem. Soc. 142 (2020) 3736–3741.
[31] R. Wang, X. Shi, Z. Zhang, A. Xiao, S.-P. Sun, Z. Cui, Y. Wang, Unidirectional diffusion synthesis of covalent organic frameworks (COFs) on polymeric substrates for dye separation, J. Membr. Sci. 586 (2019) 274–280.
[32] N. Wang, X. Li, L. Wang, L. Zhang, G. Zhang, S. Ji, Nanoconfined zeolitic imidazolate framework membranes with composite layers of nearly zero thickness, ACS Appl. Mater. Interfaces 8 (2016) 21979–21983.
[33] C. Yin, S. Fang, X. Shi, Z. Zhang, Y. Wang, Pressure-modulated synthesis of self-repairing covalent organic frameworks (COFs) for high-flux nanofiltration, J. Membr. Sci. 618 (2021) 118727.
[34] J.-X. Guo, H.-L. Qian, X. Zhao, C. Yang, X.-P. Yan, In situ room-temperature fabrication of a covalent organic framework and its bonded fiber for solid-phase microextraction of polychlorinated biphenyls in aquatic products, J. Mater. Chem. 7 (2019) 13249–13255.
[35] S.Y. Ding, J. Gao, Q. Wang, Y. Zhang, W.G. Song, C.Y. Su, W. Wang, Construction of covalent organic framework for catalysis: Pd/COF-LZU1 in Suzuki-Miyaura coupling reaction, J. Am. Chem. Soc. 133 (2011) 19816–19822.
[36] F. Pan, W. Guo, Y. Su, N.A. Khan, H. Yang, Z. Jiang, Direct growth of covalent organic framework nanofiltration membranes on modified porous substrates for dyes separation, Separ. Purif. Technol. 215 (2019) 582–589.
[37] Z. Wang, Z. Si, D. Cai, G. Li, S. Li, P. Qin, Synthesis of stable COF-300 nanofiltration membrane via in-situ growth with ultrahigh flux for selective dye separation, J. Membr. Sci. 615 (2020) 118466.
[38] Y. Hu, J. Wei, Y. Liang, H. Zhang, X. Zhang, W. Shen, H. Wang, Zeolitic imidazolate framework/graphene oxide hybrid nanosheets as seeds for the growth of ultrathin molecular sieving membranes, Angew. Chem. Int. Ed. 55 (2016) 2048–2052.
[39] Y.-Y. Su, X. Yan, Y. Chen, X.-J. Guo, X.-F. Chen, W.-Z. Lang, Facile fabrication of COF-LZU1/PES composite membrane via interfacial polymerization on microfiltration substrate for dye/salt separation, J. Membr. Sci. 618 (2021) 118706.
[40] G. Kong, J. Pang, Y. Tang, L. Fan, H. Sun, R. Wang, S. Feng, Y. Feng, W. Fan, W. Kang, H. Guo, Z. Kang, D. Sun, Efficient dye nanofiltration of a graphene oxide membrane via combination with a covalent organic framework by hot pressing, J. Mater. Chem. 7 (2019) 24301–24310.
[41] H. Wang, L. Chen, H. Yang, M. Wang, L. Yang, H. Du, C. Cao, Y. Ren, Y. Wu, F. Pan, Z. Jiang, Brønsted acid mediated covalent organic framework membranes for efficient molecular separation, J. Mater. Chem. 7 (2019) 20317–20324.
[42] N.A. Khan, R. Zhang, H. Wu, J. Shen, J. Yuan, C. Fan, L. Cao, M.A. Olson, Z. Jiang, Solid-vapor interface engineered covalent organic framework membranes for molecular separation, J. Am. Chem. Soc. 142 (2020) 13450–13458.
[43] T. Wang, H. Wu, S. Zhao, W. Zhang, M. Tahir, Z. Wang, J. Wang, Interfacial polymerized and pore-variable covalent organic framework composite membrane for dye separation, Chem. Eng. J. 384 (2020) 123347.
[44] J. Liu, G. Han, D. Zhao, K. Lu, J. Gao, T.-S. Chung, Self-standing and flexible covalent organic framework (COF) membranes for molecular separation, Sci. Adv. 6 (2020), eabb1110.
[45] D.B. Shinde, L. Cao, A.D. Dinga Wonanke, X. Li, S. Kumar, X. Liu, M.N. Hedhili, A.-H. Emwas, M. Addicoat, K.-W. Huang, Z. Lai, Pore engineering of ultrathin covalent organic framework membranes for organic solvent nanofiltration and molecular sieving, Chem. Sci. 11 (2020) 5434–5440.
[46] H. Fan, J. Gu, H. Meng, A. Knebel, J. Caro, High-flux membranes based on the covalent organic framework COF-LZU1 for selective dye separation by nanofiltration, Angew. Chem. Int. Ed. Engl. 57 (2018) 4083–4087.
[47] X.-l. Wang, W. Qin, L.-x. Wang, K.-y. Zhao, H.-c. Wang, H.-y. Liu, J.-f. Wei, Desalination of dye utilizing carboxylated TiO_2/calcium alginate hydrogel nanofiltration membrane with high salt permeation, Separ. Purif. Technol. 253 (2020) 117475.
[48] S. Liu, Z. Wang, M. Ban, P. Song, X. Song, B. Khan, Chelation-assisted in situ self-assembly route to prepare the loose PAN-based nanocomposite membrane for dye desalination, J. Membr. Sci. 566 (2018) 168–180.
[49] W. Ye, J. Lin, R. Borrego, D. Chen, A. Sotto, P. Luis, M. Liu, S. Zhao, C.Y. Tang, B. Van der Bruggen, Advanced desalination of dye/NaCl mixtures by a loose nanofiltration membrane for digital ink-jet printing, Separ. Purif. Technol. 197 (2018) 27–35.
[50] X. Chu, X. Dou, R. Liang, M. Li, W. Kong, X. Yang, J. Luo, M. Yang, M. Zhao, A self-assembly aptasensor based on thick-shell quantum dots for sensing of ochratoxin A, Nanoscale 8 (2016) 4127–4133.